

Data Repository Item

METHODS

Fossil collection. In the first instance, a 4 m² excavation area consisting of four 1 m by 1 m squares was gridded off with pegs and stringline, and a datum point established (a large metal peg embedded in an overhanging wall). Several smaller peripheral grids were then added as the excavation proceeded, using standard paleontological methods, and in 10-cm levels within units. Depths relative to datum and positions were recorded for all large fossils and significant sedimentary features (e.g., contacts between units). Digital photographs of were taken as bones were relieved out of the sediment, and sketches of bone distributions were made at each level. Larger bones were wrapped in tissue paper, labeled with field number (details recorded in excavation notebooks) and removed from the caves in tough plastic cases. Excavated sediment was labeled and removed from the cave for wet-sieving. Resultant residues of small vertebrate elements and fragments of larger vertebrate bones were then dried and sorted (picked) for taxonomically identifiable remains. Larger bones were cleaned, dried and stabilized with polyvinyl butyrate dissolved in acetone. Specimens are registered with the Department of Palaeontology, South Australian Museum, Adelaide, and housed in the on-site NCWHA Palaeontology Laboratory.

Paleoecology. Numbers of identifiable specimens (NISP) for each species were recorded in spreadsheets according to grid, level and unit. Mammals were divided into two size groups for comparisons (small, <5 kg mean body mass; large, >5 kg), although no mammals in the 4.5–13 kg range are actually present in the Cathedral Cave deposit (Tables S1–S3). Calculation of the minimum numbers of individuals (MNI) within assemblages or stratigraphic layers is a widely used method of assessing abundances of fossil species. It is an estimate of the lowest number of animals that would account for all identified specimens of a species. Here, it is a measure of the most abundant of four elements: left or right maxillary specimen, or left or right dentary specimen. Because of the varying

taphonomic pathways and subsequent disparity in sample sizes for small and large mammals, we employ MNI for examining trends in relative abundances of small species and NISP for large mammals. Employing NISP for small mammals and MNI for large mammals provides fundamentally similar results, but NISP overestimates the abundance of common taxa and MNI overestimates the abundance of rare taxa, blurring the trends we are seeking to reveal. Relative abundance ($\text{MNI}_{\text{species}}/\text{MNI}_{\text{total}} \%$, or $\text{NISP}_{\text{species}}/\text{NISP}_{\text{total}} \%$) is the most widely utilized measure of species incidence.

Variations in fossil samples sizes for different stratigraphic levels or sites greatly influence determinations of species richness (Raup, 1974; Barnosky et al., 2004, 2005). Rarefaction analysis using Analytic Rarefaction version 1.3 developed by Steven M. Holland (<http://www.uga.edu/strata/software/>) was undertaken (Fig. S1) to examine the influence of sample size differences in species richness values obtained for small mammals in the Cathedral Cave units (large mammals samples sizes are too low for rarefaction analysis to be useful). Since the lowest NISP was recorded for Unit 3 (NISP = 290), we used this value for all units to produce a standardized plot of expected species richness for small mammals through the sequence (see main text).

Chronology. Optical dating provides an estimate of the time elapsed since luminescent minerals, such as quartz, were last exposed to sunlight (Aitken, 1998; Bøtter-Jensen et al., 2003). Buried grains will accumulate the effects of the nuclear radiation flux to which they are exposed, and the burial dose (paleodose) can be measured using the optically stimulated luminescence (OSL) signal. Optical ages (Table S4) were calculated from the paleodose, measured using the OSL signal, divided by the dose rate due to ionizing radiation. We extracted quartz grains of 90–125 μm diameter from the sediment samples under dim red illumination using standard procedures, including etching by hydrofluoric acid to remove the external alpha-dosed layer (Aitken, 1998). Paleodoses were obtained from aliquots each composed of ~80 grains (to check for insufficient bleaching of the quartz grains at deposition), using the single-aliquot regenerative-dose protocol, statistical models and experimental apparatus described

elsewhere (Galbraith et al., 1999; Olley et al., 2004). Aliquots were stimulated by $\sim 10 \text{ mW cm}^{-2}$ of blue (470 nm) light for 100 s at 125°C, after a preheat of 240°C for 10 s (or a cut-heat to 160°C for test doses), and paleodoses were determined from the first 3 s of ultraviolet OSL, using the final 30 s as background. Under these conditions, correct dose estimates were obtained for aliquots that had been bleached and then given a known dose. The paleodose distributions had overdispersion values well within the range reported for single aliquots composed of well-bleached quartz (Galbraith et al., 2005), so we used the central age model (Galbraith et al., 1999) to calculate the weighted mean paleodose for each sample. A pulsed-irradiation regeneration technique (Bailey, 2004) was also tested on samples NC1 and NC2, and no reduction was achieved in the single-aliquot paleodose estimates, their precisions, or the level of scatter between aliquots. The total dose rate for each sample was calculated as the sum of the beta and gamma dose rates due to ^{238}U , ^{235}U and ^{232}Th (and their decay products) and ^{40}K (making allowance for beta-dose attenuation and sample water content), plus the cosmic-ray contribution (Prescott and Hutton, 1994) and the effective internal alpha dose rate, estimated at 0.03 Gy ka^{-1} from measurements made previously on quartz grains from southeastern Australia (Bowler et al., 2003).

For a detailed description of the analytical procedure used for U-Th dating (data presented in Table S5), see Hellstrom (2003).

Sedimentology. Fourteen sediment samples (hand-specimen size) that exemplify the Cathedral Cave sequence were collected from the faces of the excavation (Fig. S2). Friable samples were partly consolidated in situ using Araldite® epoxy resin LC191 catalyzed with hardener HY951, before removal to the surface for further processing. After air-drying, and progressively as the samples were cut up with a diamond wheel, further consolidation was carried out with the objective of filling intergranular pores as fully as possible. From each sample, a vertical face was lapped smooth for macroscopic examination, and one or more chips cut for the manufacture of standard petrographic thin-sections for optical microscopy. Lapped faces were sprayed with lacquer (Westart Crystal Clear) to

preserve the surface and to enhance color contrast. Munsell® colors were determined from these surfaces, which approximate the appearance of wet sediment.

Observations on the depositional, textural and compositional attributes of each stratigraphic unit (Figs. S3–S7) were used to develop a general model of the depositional system that produced the Cathedral Cave sediments. The model takes into account the geographic and stratigraphic setting, and the likely qualitative geochemical and clastic sedimentological responses of the system to variation in effective precipitation. The model is founded upon conceptualizations of the influence of plant growth on terrigenous sediment yields (Schumm, 1968). A recent study of an Oligocene non-marine carbonate deposit from central Australia (Megirian et al., 2004) considered the influence of effective precipitation (the major controlling influence on plant growth) on the formation, mobilization, deposition, and long-term preservation of calciclastic particles under sub-aerial exposure conditions (e.g., Esteban and Klappa, 1983), with reference to pedogenic processes and the formation of duricrusts. Although predominantly siliciclastic, the Cathedral Cave sediments contain some detrital carbonate, and both carbonate and siliciclastic formations, and pedogenic duricrust are present in the basement complex, justifying a similar interpretative approach.

Samples and thin-sections are lodged in the Vertebrate Palaeontology Laboratory of the Naracoorte Caves World Heritage Area, Naracoorte, South Australia.

FAUNAL DATA

Table S1. The Pleistocene mammal fauna from Cathedral Cave, Naracoorte Caves World

Heritage Area (excluding Microchiroptera)

Tachyglossidae	Palorchestidae	<i>Macropus</i> sp. nov.‡
<i>Tachyglossus aculeatus</i>	<i>Palorchestes azael</i> ‡	<i>Onychogalea lunata</i> †
Thylacinidae	Diprotodontidae	<i>Protemnodon</i> sp. cf. <i>brehus</i> ‡
<i>Thylacinus cynocephalus</i> †	<i>Zygomaturus trilobus</i> ‡	<i>Wallabia bicolor</i>
Dasyuridae	Thylacoleonidae	<i>Sthenurus andersoni</i> ‡
<i>Antechinus agilis</i> *	<i>Thylacoleo carnifex</i> ‡	<i>Metasthenurus newtonae</i> ‡
<i>Antechinus flavipes</i>	Acrobatidae	<i>Procoptodon goliah</i> ‡
<i>Antechinus minimus</i>	<i>Acrobates pygmaeus</i> *	" <i>Procoptodon</i> " <i>browneorum</i> ‡
<i>Antechinus swainsonii</i> *	Burramyidae	" <i>Procoptodon</i> " <i>gilli</i> ‡
<i>Dasyurus maculatus</i> *	<i>Cercartetus lepidus</i>	<i>Simosthenurus maddocki</i> ‡
<i>Dasyurus viverrinus</i> *	<i>Cercartetus nanus</i>	<i>Simosthenurus occidentalis</i> ‡
<i>Ningui yvonnae</i> *	Petauridae	" <i>Simosthenurus</i> " <i>pales</i> ‡
<i>Phascogale calura</i> *	<i>Petaurus breviceps</i>	Muridae
<i>Phascogale tapoatafa</i>	Pseudocheiridae	<i>Conilurus albipes</i> †
<i>Sarcophilus lanarius</i> ‡	<i>Pseudocheirus peregrinus</i>	<i>Hydromys chrysogaster</i>
<i>Sminthopsis crassicaudata</i>	Phalangeridae	<i>Mastacomys fuscus</i> *
<i>Sminthopsis murina</i>	<i>Trichosurus vulpecula</i>	<i>Notomys mitchellii</i>
Peramelidae	Macropodidae	<i>Pseudomys apodemoides</i>
<i>Isoodon obesulus</i>	<i>Bettongia gaimardi</i> *	<i>Pseudomys auritus</i> †
<i>Perameles bougainville</i> *	<i>Bettongia penicillata</i> *	<i>Pseudomys australis</i> *
<i>Perameles gunnii</i> *	<i>Potorous platyops</i> †	<i>Pseudomys fumeus</i> *
Phascolarctidae	<i>Potorous tridactylus</i> *	<i>Pseudomys gouldii</i> †
<i>Phascolarctos stirtoni</i> ‡	<i>Lagorchestes leporides</i> †	<i>Pseudomys shortridgei</i>
Vombatidae (wombats)	<i>Macropus giganteus</i>	<i>Rattus fuscipes</i> *
<i>Lasiorhinus krefftii</i> *	<i>Macropus greyi</i> †	<i>Rattus lutreolus</i>
<i>Vombatus ursinus</i>	<i>Macropus rufogriseus</i>	<i>Rattus tunneyi</i> *

* Locally extinct; † Completely extinct in late Holocene; ‡ Completely extinct in late Pleistocene. All other species inhabit the region today.

Table S2. Cathedral Cave large mammal relative abundance data.

Species	Body Mass* (kg)	Relative Abundance (NISP _{species} /NISP _{total} %)					Last Dated Local Occurrence (ka ago)
		Unit	Unit	Unit	Unit	Unit	
		4	3	2b	2a	1	
<i>Phascolarctos stirtoni</i>	13	7.7	10.2	1.4	0.0	0.0	84±7 ¹
<i>Macropus greyi</i>	13	3.8	10.2	2.7	0.0	5.0	<0.1 ²
<i>Wallabia bicolor</i>	15	23.1	6.1	8.1	7.7	0.0	Still in area
<i>Macropus rufogriseus</i>	16	80.8	34.7	14.9	7.7	25.0	Still in area
<i>Sarcophilus lanarius</i>	19	7.7	2.0	0.0	0.0	0.0	>49 ³
<i>Macropus</i> sp. nov.	23	3.8	0.0	0.0	0.0	0.0	~535,000 ⁴
<i>Thylacinus cynocephalus</i>	25	0.0	2.0	1.4	0.0	5.0	<0.1 ²
<i>Vombatus ursinus</i>	26	3.8	2.0	1.4	0.0	10.0	Still in area
" <i>Procoptodon</i> " <i>gilli</i>	30	11.5	30.6	45.9	30.8	5.0	84±7 ¹
<i>Lasiorhinus krefftii</i>	31	3.8	2.0	0.0	0.0	0.0	~280 ⁴
<i>Macropus giganteus</i>	49	23.1	12.2	27.0	30.8	45.0	Still in area ⁵
<i>Sthenurus andersoni</i>	50	19.2	2.0	0.0	0.0	0.0	84±7 ^{1,6}
<i>Simosthenurus maddocki</i>	50	0.0	0.0	4.1	7.7	0.0	84±7 ^{1,6}
<i>Simosthenurus occidentalis</i>	50	11.5	8.2	4.1	0.0	0.0	84±7 ^{1,6}
<i>Metasthenurus newtonae</i>	55	11.5	4.1	1.4	0.0	0.0	84±7 ¹
" <i>Procoptodon</i> " <i>browneorum</i>	60	3.8	12.2	4.1	0.0	0.0	84±7 ¹
<i>Protemnodon</i> sp. cf. <i>brehus</i>	100	3.8	8.2	1.4	0.0	0.0	45±2 ^{3,7}
<i>Thylacoleo carnifex</i>	104	3.8	4.1	1.4	7.7	5.0	84±7 ¹
" <i>Simosthenurus</i> " <i>pales</i>	150	0.0	0.0	1.4	0.0	0.0	~280 ⁴
<i>Procoptodon goliah</i>	250	0.0	2.0	2.7	15.4	25.0	~206 ⁴
<i>Palorchestes azael</i>	500	0.0	0.0	1.4	0.0	0.0	~280 ⁴
<i>Zygomaturus trilobus</i>	500	3.8	10.2	2.7	7.7	5.0	44–47 ³
No. Large Species	16	18	18	8	9		
No. Species Megafauna	10	10	12	5	4		
No. Species Non-megafauna	6	7	6	3	5		
NISP All Large Species	59	80	94	15	26		
NISP Megafauna	23	46	53	9	8		
NISP Non-megafauna	36	34	41	6	18		
Density All Large Species	67.0	92.0	62.3	12.5	22.6		
Density Megafauna	26.1	52.9	35.1	7.5	7.0		
Density Non-megafauna	40.9	39.1	27.2	5.0	15.7		
Sediment Volume (m ³)	1.15	1.20	1.51	0.87	0.88		

* Mean body masses derived from Strahan (1995) for extant species and Johnson and Prideaux (2004) for extinct species, except *Thylacoleo carnifex* for which Wroe et al. (2004) was used.

¹ From Reed and Bourne (2000) and Roberts et al. (2001). The last dated occurrence of the megafaunal snake, *Wonambi naracoortensis*, is also 84 ± 7 ka.

² From Strahan (1995).

³ From McDowell (2001).

⁴ This study.

⁵ *Macropus fuliginosus*, which is osteologically inseparable from *M. giganteus*, still lives in the area. We follow the usual convention of referring Pleistocene occurrences in southeastern Australia to *M. giganteus*.

⁶ From Gresham (2000).

⁷ *Protemnodon* sp. cf. *brehus* has been recorded in two strata with younger ages (McDowell, 2001), but each record represents one individual tooth, both of which may easily have been reworked from older strata.

Table S3. Cathedral Cave small mammal relative abundance data.

Species	Body Mass* (kg)	Relative Abundance (MNI _{species} /MNI _{total} %)					Last Dated Local Occurrence (ka ago)
		Unit	Unit	Unit	Unit	Unit	
		4	3	2b	2a	1	
<i>Acrobates pygmaeus</i>	0.01	0.0	0.8	0.1	0.0	0.0	Still in area
<i>Cercartetus lepidus</i>	0.01	1.9	1.6	6.8	1.7	0.8	Still in area
<i>Ningau yvonnae</i>	0.01	0.5	0.0	0.1	0.0	0.0	8,080 ¹
<i>Antechinus agilis</i>	0.02	0.0	0.0	0.4	0.4	0.5	~206,000 ²
<i>Cercartetus nanus</i>	0.02	6.1	8.8	8.1	5.0	4.1	Still in area
<i>Sminthopsis crassicaudata</i>	0.02	23.1	16.0	48.7	39.7	23.9	Still in area
<i>Sminthopsis murina</i>	0.02	2.8	0.8	1.5	0.4	0.5	Still in area
<i>Pseudomys apodemoides</i>	0.02	1.4	3.2	2.4	2.5	1.3	Still in area
<i>Antechinus flavipes</i>	0.04	5.2	3.2	1.9	0.8	0.5	Still in area
<i>Pseudomys gouldii</i>	0.05	0.0	0.0	0.0	0.4	0.0	<740 ¹
<i>Antechinus minimus</i>	0.05	0.5	0.0	0.0	0.0	0.0	Still in area
<i>Antechinus swainsonii</i>	0.05	0.9	0.0	0.0	0.0	0.0	~535,000 ²
<i>Notomys mitchellii</i>	0.05	0.0	2.4	0.1	0.4	0.0	Still in area
<i>Phascogale calura</i>	0.05	0.0	0.0	0.0	0.0	0.5	~206,000 ²
<i>Pseudomys australis</i>	0.07	7.5	9.6	8.3	17.4	24.7	<740 ¹
<i>Pseudomys fumeus</i>	0.07	10.8	13.6	2.2	1.2	0.5	1,010 ¹
<i>Pseudomys shortridgei</i>	0.07	0.9	3.2	0.4	1.2	1.0	<740 ¹
<i>Pseudomys auritus</i>	0.09	10.8	12.8	2.2	7.4	13.0	<740 ¹
<i>Rattus lutreolus</i>	0.11	0.0	0.0	0.1	0.0	0.3	Still in area
<i>Mastacomys fuscus</i>	0.12	7.1	7.2	4.6	7.9	11.5	<740 ¹
<i>Rattus tunneyi</i>	0.12	0.5	0.8	2.2	3.3	2.0	<740 ¹
<i>Petaurus breviceps</i>	0.13	0.5	0.0	0.3	0.0	0.0	Still in area
<i>Rattus fuscipes</i>	0.14	0.5	0.0	0.4	0.4	0.0	Still in area
<i>Phascogale tapoatafa</i>	0.19	0.0	0.0	0.1	0.0	0.0	Still in area
<i>Conilurus albipes</i>	0.20	0.5	0.0	0.0	0.0	0.3	<200 ³
<i>Perameles bougainville</i>	0.23	8.0	3.2	4.4	3.7	4.1	<740 ⁴
<i>Hydromys chrysogaster</i>	0.69	0.5	0.0	0.1	0.4	0.0	Still in area
<i>Potorous platyops</i>	0.74	0.0	0.8	0.4	0.4	0.8	<740 ¹
<i>Isodon obesulus</i>	0.78	0.5	0.8	0.3	0.4	0.8	Still in area
<i>Perameles gunnii</i>	0.87	1.4	0.8	0.9	2.5	2.8	<740 ¹
<i>Pseudocheirus peregrinus</i>	0.90	0.9	0.8	0.6	0.8	1.0	Still in area
<i>Dasyurus viverrinus</i>	1.1	0.9	0.8	0.3	0.4	1.5	<740 ¹
<i>Potorous tridactylus</i>	1.1	3.8	6.4	0.9	1.2	2.3	<740 ⁴
<i>Bettongia penicillata</i>	1.3	1.9	0.0	0.1	0.0	0.3	~206,000 ²
<i>Bettongia gaimardi</i>	1.7	0.0	0.8	0.3	0.0	0.5	<200 ³
<i>Dasyurus maculatus</i>	2.7	0.0	0.0	0.0	0.0	0.3	<150 ⁵
<i>Lagorchestes leporides</i>	3.1	0.0	0.0	0.1	0.0	0.3	<150 ⁵
<i>Onychogalea lunata</i>	3.5	0.5	0.0	0.0	0.0	0.0	<740 ⁴

<i>Trichosurus vulpecula</i>	4.0	0.0	0.8	0.1	0.0	0.3	Still in area
<i>Tachyglossus aculeatus</i>	4.5	0.0	0.8	0.0	0.0	0.0	Still in area
No. Small Species	27	24	32	24	28		
MNI All Small Species	212	125	677	242	393		

* Mean body masses derived from Strahan (1995).

¹ From McDowell (2001).

² This study.

³ From Strahan (1995).

⁴ Personal re-identification by GJP of specimens listed in McDowell (2001).

⁵ South Australian Museum records.

Note: Last Dated Local Occurrences for some species (e.g., *Antechinus swainsonii*, *Bettongia penicillata*) almost certainly do not reflect their most recent occurrence in the region, but a lack of dated late Pleistocene to Holocene sites.

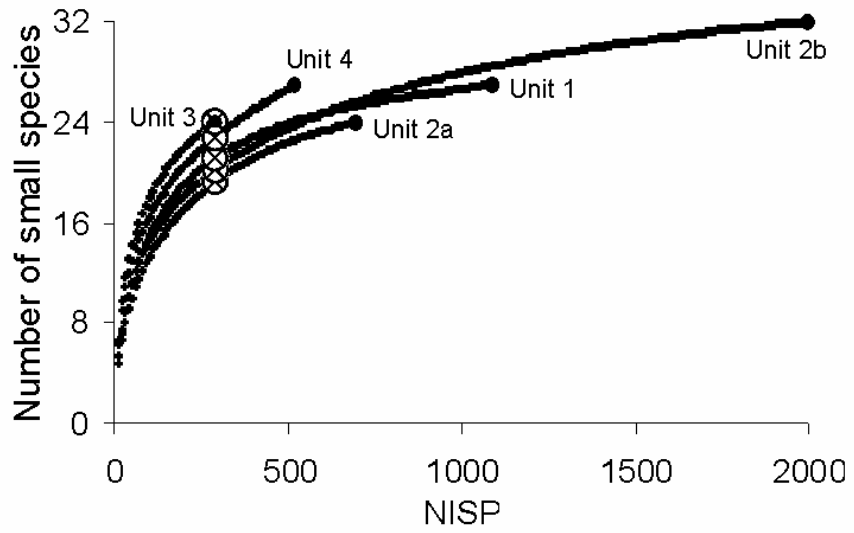


Figure S1. Rarefaction curves for small species for each unit. Open crossed circles denote NISP = 290.

CHRONOLOGIC DATA

Table S4. Dose rate data, paleodoses and optical ages for sediment samples from Cathedral Cave, Naracoorte, South Australia.

Sample code	Unit / Depth below datum (cm)	Water content ^a (%)	Radionuclide activities ^b (Bq kg ⁻¹)						Cosmic-ray dose rate ^c (Gy ka ⁻¹)	Total dose rate ^d (Gy ka ⁻¹)	Paleodose ^d (Gy)	Number of aliquots / σ ^e (%)	Optical age ^d (ka)
			²³⁸ U	²²⁶ Ra	²¹⁰ Pb	²²⁸ Ra	²²⁸ Th	⁴⁰ K					
NC1	1 / 102	35	11.7 ± 1.9	12.7 ± 0.2	11.1 ± 1.8	44.7 ± 0.6	44.8 ± 0.3	179 ± 3	0.071	1.26 ± 0.04	260 ± 19	12 / 0	206 ± 16
NC2	2a / 114	16	8.8 ± 1.2	8.5 ± 0.2	8.1 ± 1.8	27.4 ± 0.5	27.8 ± 0.3	103 ± 3	0.070	0.95 ± 0.04	220 ± 18	11 / 11	231 ± 21
NC3	2b / 134	23	10.7 ± 2.2	11.7 ± 0.2	9.3 ± 1.6	50.9 ± 0.7	52.0 ± 0.4	160 ± 4	0.069	1.42 ± 0.05	364 ± 28	11 / 11	257 ± 21
NC4	3 / 165	15	11.6 ± 1.2	9.6 ± 0.1	7.1 ± 1.0	39.5 ± 0.3	39.7 ± 0.2	116.4 ± 1.7	0.068	1.19 ± 0.04	355 ± 20	15 / 12	292 ± 19
NC5	4 / 190	4	7.0 ± 1.0	7.4 ± 0.1	8.5 ± 0.7	12.4 ± 0.2	12.7 ± 0.1	51.7 ± 1.1	0.065	0.63 ± 0.02	325 ± 44	9 / 11	513 ± 73
NC6	4 / 185	4	4.4 ± 0.8	5.5 ± 0.1	5.9 ± 0.7	11.2 ± 0.2	11.1 ± 0.1	55.7 ± 1.2	0.065	0.57 ± 0.02	305 ± 25	11 / 0	535 ± 49

^a Measured (field) water content (expressed as % of dry mass of sample) used for dose rate and age calculations, with an assigned uncertainty of ± 2%.

^b Measurements made on dried and powdered samples by high-resolution gamma-ray spectrometry. These show that the ²³⁸U and ²³²Th decay series are both presently in secular equilibrium. Concentrations of 1 p.p.m. ²³⁸U, 1 p.p.m. ²³²Th and 1% ⁴⁰K correspond to activities of 12.4, 4.1 and 316 Bq kg⁻¹, respectively.

^c Estimates for dry samples (corrected for site altitude, geomagnetic latitude, and thickness of rock and sediment overburden) and assigned uncertainties of ± 10%.

^d Mean ± total uncertainty (68% confidence interval), calculated as the quadratic sum of random and systematic uncertainties. Paleodose uncertainty includes a systematic component of ± 2% associated with laboratory beta-source calibration.

^e Number of aliquots used for paleodose determination, together with estimate of overdispersion (σ , the relative standard deviation of the apparent paleodoses after allowing for measurement uncertainties).

Table S5. U-Th data for the flowstone separating Units 4 and 3 within the Cathedral Cave sequence. $[\text{}^{230}\text{Th}/\text{}^{238}\text{U}]$ and $[\text{}^{234}\text{U}/\text{}^{238}\text{U}]$ denote activity ratios relative to the HU-1 equilibrium standard. Corrected age and $[\text{}^{234}\text{U}/\text{}^{238}\text{U}]_i$ ($[\text{}^{234}\text{U}/\text{}^{238}\text{U}]$ at time of formation) and their uncertainties are calculated with standard equations using the three reported activity ratios, an assumed initial $[\text{}^{230}\text{Th}/\text{}^{232}\text{Th}]$ activity of 1.5 ± 1.5 and decay constants of 9.195×10^{-6} ($\text{}^{230}\text{Th}$) and 2.835×10^{-6} ($\text{}^{234}\text{U}$). Numbers in brackets are 95% uncertainties.

Sample	U $\mu\text{g g}^{-1}$	$[\text{}^{230}\text{Th}/\text{}^{238}\text{U}]$ ($\pm 2\sigma$)	$[\text{}^{234}\text{U}/\text{}^{238}\text{U}]$ ($\pm 2\sigma$)	$[\text{}^{232}\text{Th}/\text{}^{238}\text{U}]$ ($\pm 2\sigma$)	Age ka corrected ($\pm 2\sigma$)	$[\text{}^{234}\text{U}/\text{}^{238}\text{U}]_i$ corrected ($\pm 2\sigma$)
NCF1-2 top	--	1.078(0.005)	1.118(0.003)	0.04235(0.00078)	289 \pm 10	1.268(0.007)
NCF1-3 mid	0.05	1.077(0.006)	1.116(0.003)	0.00220(0.00003)	297 \pm 9	1.269(0.007)
NCF1-1 base	--	1.139(0.004)	1.123(0.003)	0.04307(0.00049)	396 \pm 19	1.378(0.016)

PETROGRAPHY AND SEDIMENTOLOGY

Geological setting. The Naracoorte cave system is developed in the early Miocene member of the bryozoal Gambier Limestone of shallow marine origin (Wells et al., 1984). In the Naracoorte region, the Gambier Limestone is succeeded by the Parilla Sand, a littoral to near-shore marine deposit of late Pliocene age, which is composed predominantly of red-brown medium-grained quartz sand with some clay, silt and coarse sand (Wells et al., 1984; Brown and Stephenson, 1991). A ferruginous capping (ferricrete), sometimes with ferruginous pisolites, is developed locally on the Parilla Sand, which crops out principally on the eastern side of the SSE/NNW-trending Kanawinka Fault, the major structural feature of the region. To the west of this fault, the Parilla Sand is masked by a veneer of Quaternary beach sands and interdunal swamp and other deposits. The beach sands are composed almost entirely of quartz and carbonate bioclasts, which have been reported to occur in the approximate ratio of 1:3 (Banerjee et al., 2003), although there is, no doubt, variability from place to place. During the Pleistocene, the region was gently up-warped, causing the coastline to regress to the southwest, leaving behind a parallel sequence of beach dune ridges (Cook et al., 1977). The second-oldest ridge, along with its underlying strata, was differentially uplifted as a result of crustal displacements on the Kanawinka Fault. The resulting geomorphic feature, the East Naracoorte Range, runs parallel to the Kanawinka Fault, with elevated Gambier Limestone becoming a locus for karst development, of which the Naracoorte cave system is a major feature (Wells et al., 1984).

As outlined in the main text, the fossiliferous Cathedral Cave sediments evidently accumulated through a single solution pipe. The nature of the surface drainage area previously captured by this solution pipe is not known, but, in a heavily karstified terrain developed along an elevated ridge, it was most likely only ever of localized extent.

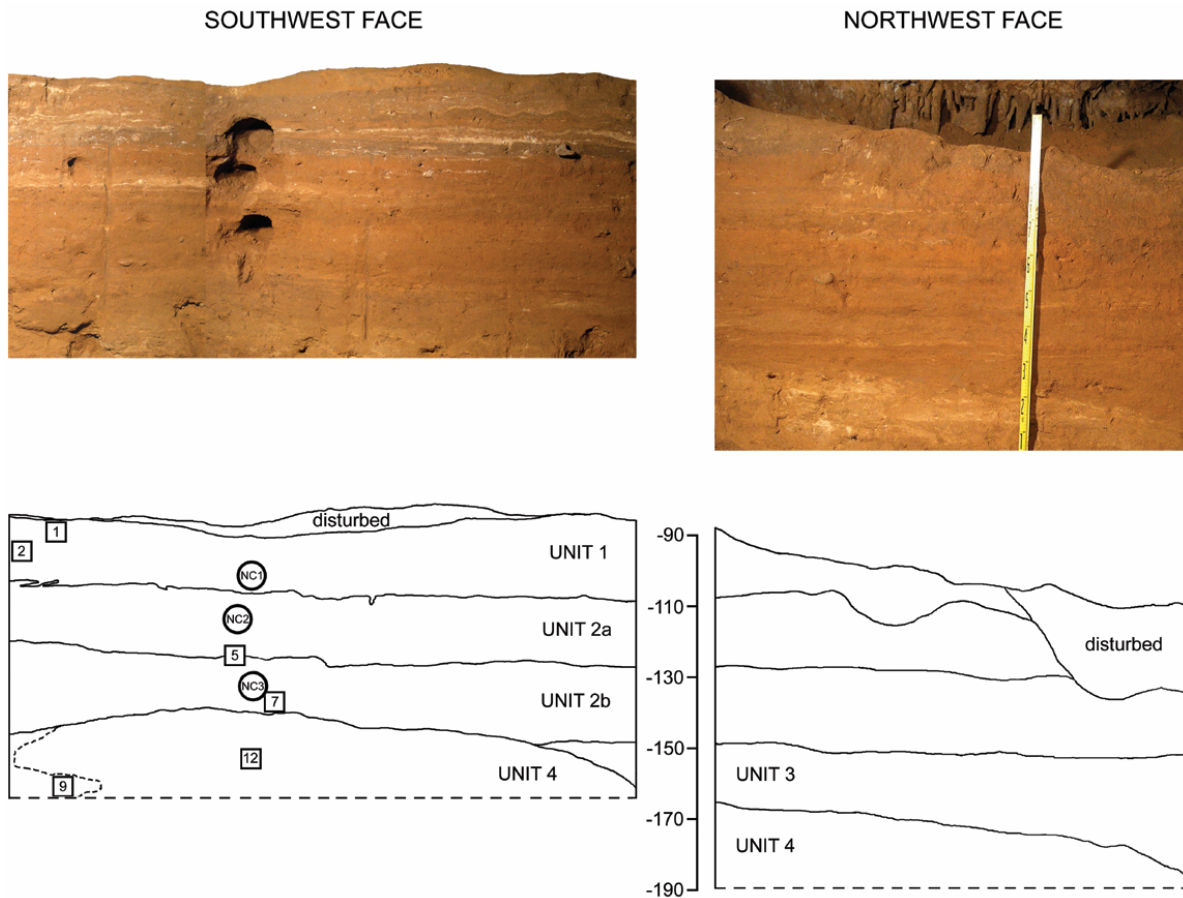


Figure S2. Photographs of the sections exposed in two faces of the 2003–2004 Cathedral Cave excavation, and their stratigraphic interpretation.

Vertical scale (centre, bottom) indicates depth (in cm) relative to datum. $^{230}\text{Th}/^{234}\text{U}$ samples were taken from a flowstone capping Unit 1 higher on the sedimentary cone (159 ± 2 ka) and another in the lower one-third of Unit 3 (279 ± 7 ka; Ayliffe et al., 1998; Moriarty et al., 2000). See Table S4 for depths of optical dating samples (NC1–6). NC1–3 were collected from the southwest face (indicated by circles); NC4–6 came from elsewhere in the excavation. Six sediment samples utilized for petrographic analysis were collected from the southwest face (indicated by numbered squares; the prefix CC is omitted); eight others came from elsewhere in the excavation.

Petrographic methods. Fourteen sediment samples (hand-specimen size) that exemplify the Cathedral Cave sequence were collected from the faces of the excavation (Fig. S2). Friable samples

were partly consolidated *in situ* using Araldite® epoxy resin LC191 catalyzed with hardener HY951, before removal to the surface for further processing. After air-drying, and progressively as the samples were cut up with a diamond wheel, further consolidation was carried out with the objective of filling intergranular pores as fully as possible. From each sample, a vertical face was lapped smooth for macroscopic examination, and one or more chips cut for the manufacture of standard petrographic thin-sections. Lapped faces were sprayed with lacquer (Westart Crystal Clear) to preserve the surface and to enhance color contrast. Munsell® colors were determined from these surfaces, which approximate the appearance of wet sediment. Specimens are lodged in the Vertebrate Palaeontology Laboratory of the Naracoorte Caves World Heritage Area, Naracoorte, South Australia.

Sediment descriptions.

Principal fabrics. The excavated Cathedral Cave sediments range texturally from silty to pebbly sands, and are composed of a relatively small number of fabrics:

1. Well-rounded quartz, typically medium- to coarse-sand grade (e.g., Fig. S3B). Such grains occur in the Gambier Limestone, Parilla Sand, and Quaternary beach deposits, implying cycles of reworking. Many isolated grains are rimmed by ferruginous clay.
2. Sub-rounded to sub-angular quartz, typically coarse-silt to fine-sand grade (e.g., Fig. S3B). Additional observations as for Fabric 1.
3. Silt- to pebble-sized ferruginous, clay-bound aggregates (e.g., Fig. S4C), typically moderate reddish brown (Munsell® 10R 4/6) or moderate brown (5YR 4/4, 3/4). They are composed of the most weathering-resistant species (e.g., kaolinite). Many of the larger clay aggregates incorporate quartz grains ranging from fine-silt to coarse-sand grade, and variously well-rounded to sub-angular (cf. quartz grains in Fabrics 1 and 2). These aggregates are inferred to have originated, at least in part, from the Parilla Sand or from its alluvial or pedogenic derivatives. Ferruginous pisolites (laterite pebbles) support the idea that the Parilla Sand is a source, directly or indirectly, for these aggregates.

4. Red-brown clay and micro-detrital clayey particles (e.g., Figs. S4B–C). These fines are interpreted to have also originated from the Parilla Sand and/or its derivatives, and typically occupy intergranular voids between coarser (i.e., sand and silt grade) fabrics.
5. Carbonate lithoclasts of sand to pebble grade, variously preserving palimpsests of marine fossils or composed of pseudospar (e.g., Figs. S4C, S5C–E, S7I–J) or more rarely, dense micrite (Fig. S6F). Both are believed to originate primarily from the Gambier Limestone, in which recrystallization is a common feature.
6. Chert (chalcedonic) grains (e.g., Figs. S5D, S7I–J). These probably also originate from the Gambier Limestone, which in places contains flint nodules.
7. Phosphatic bioclasts; i.e., bones and bone fragments (e.g., Figs. S6B, S7E).
8. Charcoal, ranging from fine-silt to pebble-sized fragments (e.g., Fig. S5E).
9. Diagenetic carbonate cements (e.g., Figs. S3E–F, S5B,C,K).
10. Diagenetic phosphatic cements (e.g., Fig. S3C–D).
11. Minor autochthonous grains including reworked fabrics (e.g., Fig. S7G–H) and large carbonate clasts (Gambier Limestone) that most likely represent roof falls rather than transported allochthonous grains.

Characterization of the depositional units. Units 4–1, and sedimentary facies within them, are distinguishable by the relative frequencies of the various fabrics and textural attributes. Although some relative abundances are quoted below, these are merely indicative, and the focus is on how the various units differ qualitatively. It is evident, even at the scale of photographs of the faces of the Cathedral Cave excavation, that there is significant lateral and considerable vertical heterogeneity within the differentiated depositional units (e.g., Fig. S2), and this is apparent also at the hand-specimen and microscopic scales. Fields of view shown in photomicrographs (Figs. S3–S7) were selected to show the general nature of textural and compositional differences between the differentiated sedimentary units.

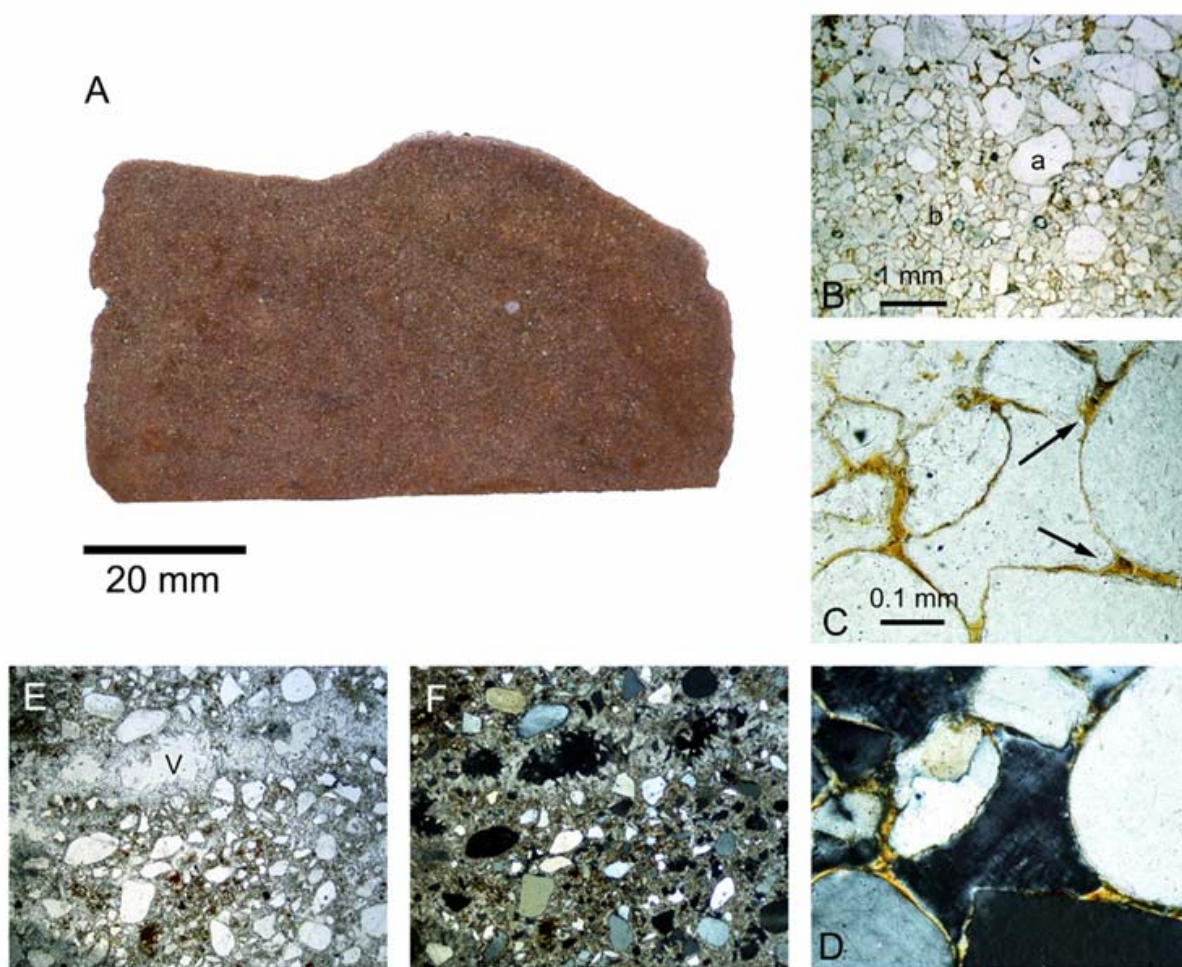


Figure S3. Unit 4 petrographic photomicrographs. A: Sample CC12 slabbed face. B: Bimodal quartz sand composed of a, well-rounded coarse grains, and b, sub-angular to sub-rounded fine grains (CC12, plane polarized light). C: CC12 (plane polarized light), diagenetic intergranular phosphate meniscus cement (arrows). D: CC12 (as for (C), crossed nicols). E: CC13B (plane polarized light), intergranular, diagenetic fine sparry calcite cement, with blocky calcite spar partially occluding a larger void (v). F: CC13B (crossed nicols). Scale bar for B applies to E and F.

UNIT 4 (Fig. S3). Unit 4 consists of moderate yellowish brown (Munsell 10YR 5/4) to dark yellowish orange (10YR 5/4), friable to weakly-consolidated bimodal quartz sand. Present only in very small quantities are sand-grade, reddish-brown, clayey or clay-bound aggregates, interstitial (disseminated) clay, charcoal and carbonate clasts. Grit- to pebble-sized clayey aggregates are rare. There is evidence in outcrop of scour and fill structures within the unit, which therefore accumulated

by a number of depositional episodes, but the different deposits within the unit are texturally and compositionally similar. Phosphatic meniscus cement (a secondary feature) is common, and in localized patches phosphate may even fully occlude primary porosity. In some samples, fine sparry calcite cement is also present. The phosphatic cement is largely responsible for the yellowish color of the unit.

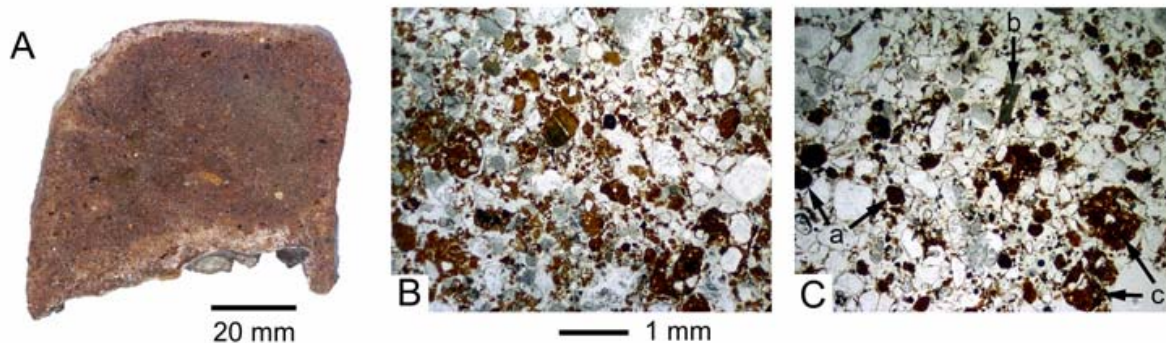


Figure S4. Unit 3 petrographic photomicrographs. A: Sample CC10 slabbed face. B: CC10 (plane polarized light), typical view showing textural attributes comparable to Unit 4. C: CC11 (plane polarized light), showing examples of ferruginous, fine-sand grade, clayey aggregates (a), carbonate grain (b), examples of coarse-sand grade ferruginous quartz-clay aggregates (c).

Scale bar for B also applies to C.

UNIT 3 (Fig. S4). Unit 3 is texturally similar to Unit 4, but differs compositionally by having a significantly higher abundance (~10–20%) of sand-grade, reddish-brown clay or clay-bound aggregates, which are sufficient to impart moderate brown hues (5YR 4/4, 3/4) to the bulk sample. Disseminated micro-detrital clay particles and carbonate clasts are also more abundant than in Unit 4, but charcoal is not markedly so. No carbonate cements were observed in thin-section, but some localized patches of phosphatic cement are present.

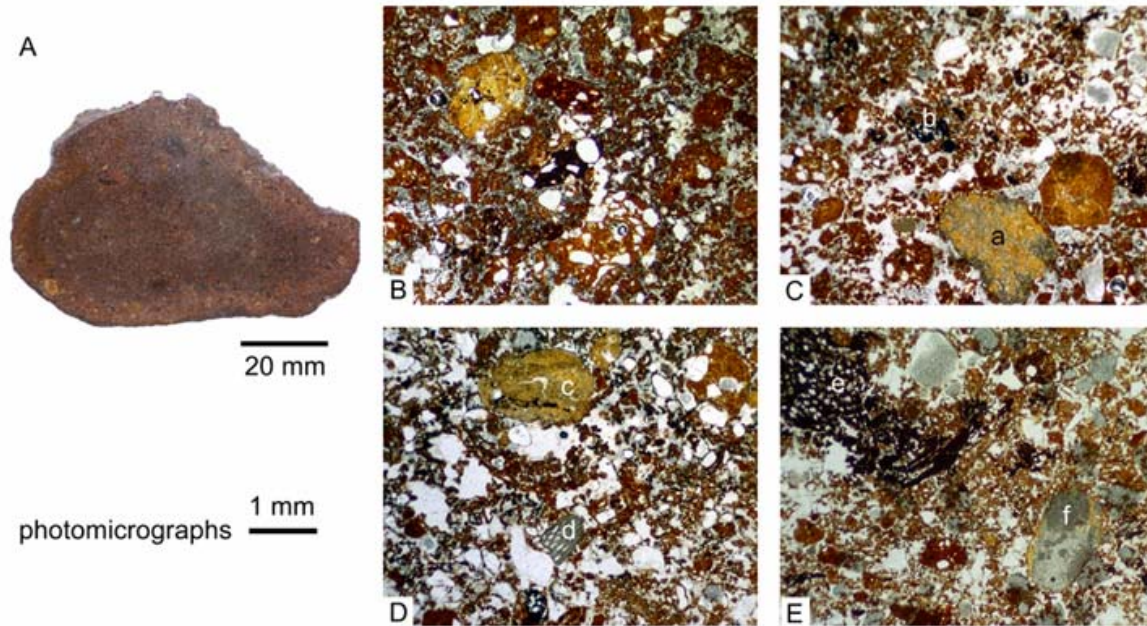


Figure S5. Unit 2b petrographic photomicrographs. A: Sample CC6 slabbed face. B,C: CC11 (plane polarized light), general views showing poor sorting and predominance of ferruginous lithoclasts over free quartz grains. Partially silicified carbonate (pseudosparite) grain (a), localized concentration of charcoal fragments (b). D,E: CC5 (plane polarized light), showing chalcedonic grain (c), probably after carbonate (compare with (a) and (f)), bryozoal carbonate bioclasts (d), large charcoal particle with some of the original cellular structure recognizable (e), carbonate grain preserving palimpsests of primary features (f), with some silicification around the margins. Note that in D and E, the majority of the white areas are voids, not quartz grains.

UNIT 2b (Fig. S5). Although appearing quite massive in outcrop, Unit 2b consists of thinly bedded (2–10 cm), poorly sorted, gritty to pebbly sand beds, composed predominantly (~50–70%) of clay aggregates. The compositional variation between these beds does not, however, manifest itself as readily discerned color variations in outcrop, and the unit overall is moderate brown (5YR 4/4, 3/4) with a grayish hue, which we attribute to a significant amount of charcoal. Unit 2b is markedly more poorly sorted than Units 4 and 3, and carbonate lithoclasts and charcoal particles are significantly more abundant.

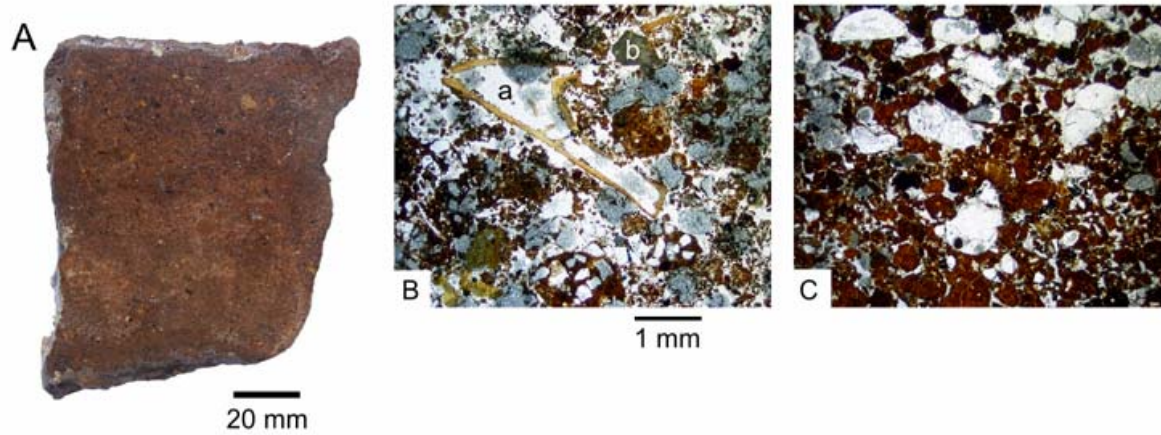


Figure S6. Unit 2a petrographic photomicrographs. A: Sample CC4 slabbed face. B: CC4 (plane polarized light), showing the poor sorting that is typical of the unit, and the preponderance of ferruginous lithoclasts over free quartz. Note that many of the white areas are voids, rather than quartz grains. Bone fragment (a), carbonate lithoclasts (b). C: CC5 (plane polarized light), showing contact (horizontal centre line) between two small-scale (~1 cm thick) comparatively well-sorted beds (upper bed rich in coarse quartz sand and lower bed rich in ferruginous lithoclasts) from the base of the unit. Such interbeds are not typical of the unit as a whole. Note that the speckled appearance of some quartz grains is an artifact of the grinding process.

UNIT 2a (Fig. S6). Unit 2a is very similar to Unit 2b in bedding and textural attributes, but overall contains fewer clay aggregates in proportion to the amount of quartz. Bedding is more readily discernible than in Unit 2b, as the comparatively quartz-rich beds are somewhat paler than those richer in clay aggregates. Carbonate lithoclasts are about as abundant as in Unit 2b. While charcoal is common, it is slightly less abundant than in Unit 2b.

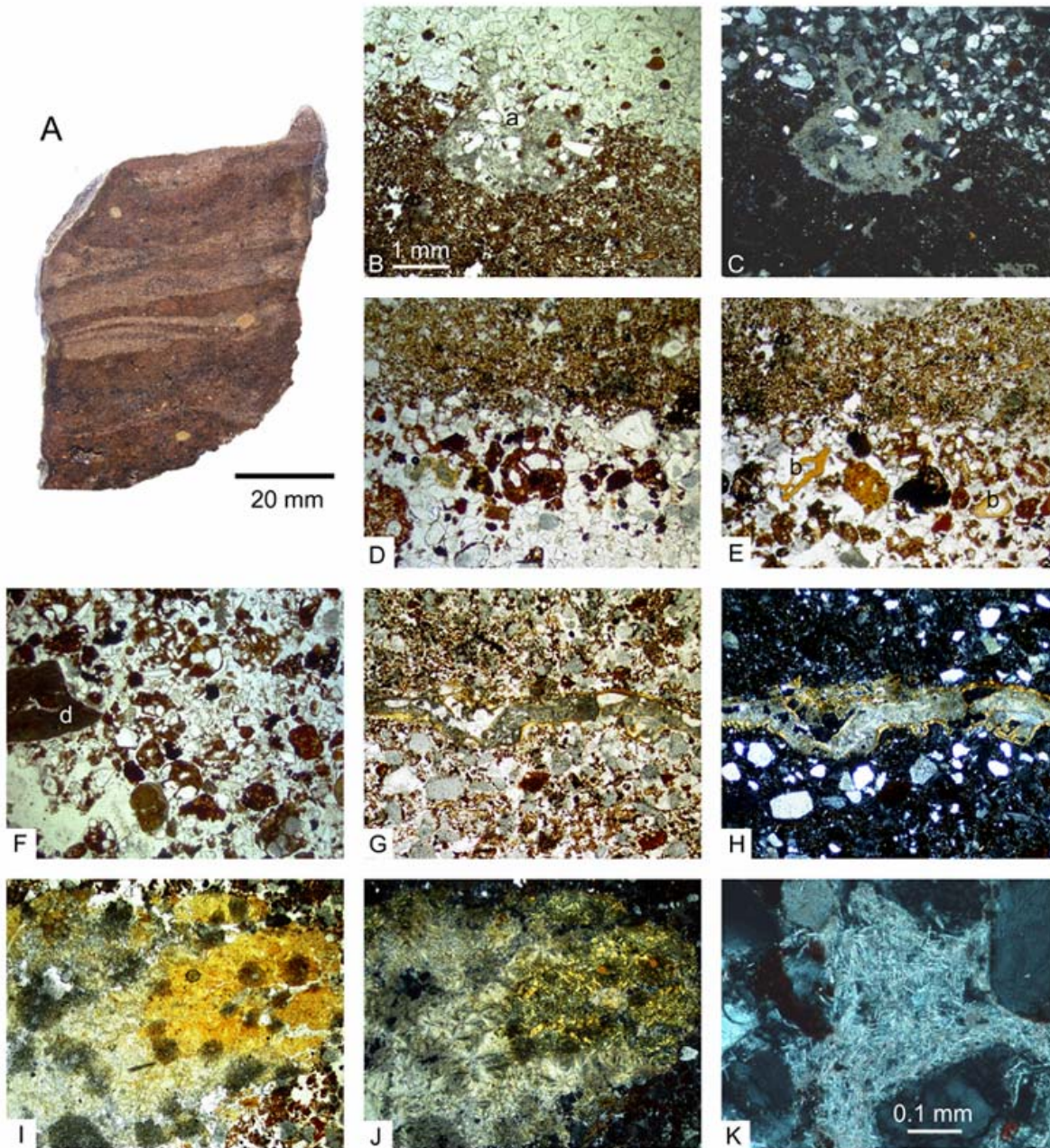


Figure S7. Unit 1 petrographic photomicrographs. A: Sample CC2 slabbed face. B: CC2 (plane polarized light), showing bedding contact between well-sorted ‘clean’ quartz sand (upper bed) comparable to that of Unit 4, and a well-sorted, charcoal-rich, coarse-silt to fine-sand grade bed composed largely of ferruginous clay aggregates (lower bed). The fabric in the centre of view (a) is cemented by needle fiber calcite cement (?aragonite), shown under higher magnification (crossed nicols) in K. Scale bar applies to all photomicrographs, except for K. C: CC2 (as for B, crossed nicols). D,E: CC2 (plane polarized light), showing the contact between the fine aggregate-rich bed seen in B and C, and the underlying, moderately-sorted, fossiliferous (b, bone fragments), coarse sandy unit comparable to Unit 3. F: CC2

(plane polarized light). View typical much of the unit, consisting of poorly-sorted gritty to pebbly sand (c, carbonate clast composed of dense micrite), with abundant ferruginous aggregates comparable to Unit 2a. Note that most of the white areas are voids, rather than quartz grains. G: CC2 (plane polarized light), elongate grain spanning the field of view on the horizontal centerline is carbonate irregularly rimmed with phosphate cement (brighter marginal zones). This was probably re-worked from within the cave environment. H: CC2 (as for G, crossed nicols). I: CC2 (plane polarized light), view of a partially silicified carbonate pebble. In plane light, the carbonate (especially bottom-right quadrant) appears as fine spar (pseudosparite), but, under crossed nicols, the carbonate exhibits elements showing pseudoradial extinction and vague, ragged crystal outlines when rotated. This is probably a remnant of a primary feature, largely obliterated by neomorphic recrystallization, followed by silicification (especially right half of the pebble). J: (as for I, crossed nicols. K: Refer to B and C.

UNIT 1 (Fig. S7). Unit 1 consists of alternating, but irregular and discontinuous, thinly-bedded (0.5–3.0 cm) pale yellowish brown (10YR 6/2) to very pale orange (10TR 8/2) clean quartz sand and moderate brown (5YR 4/4 to 5YR 3/4) aggregate-rich sand. The aggregate-rich beds are variously well sorted, comparable to Unit 3, or more poorly-sorted (gritty and pebbly), comparable to Unit 2a. Localized patches of needle fiber (?aragonite) cement are present.

Discussion and interpretation. *Theoretical basis.* From a general perspective, in a more-or-less stabilized landscape of low relief, a higher effective precipitation (approximately a function of mean annual rainfall divided by mean annual temperature) results in greater plant growth and, consequently, a more complete vegetation canopy and ground cover. The more complete the vegetation cover, the greater the interception of precipitation, the better the binding of soils by plant roots, and the thicker the humus and mulch layers. The runoff co-efficient is thus reduced. Under reduced overland flow velocities, sediment yields tend to be low, with smaller, rather than larger, detrital particles being mobilized. Chemical weathering may be favored over mechanical weathering. Conditions of higher effective precipitation tend to result in compositionally and texturally more mature alluvial deposits than those deposited under conditions of lower effective precipitation.

Cathedral Cave depositional system. The preceding descriptions include observations on diagenetic (secondary) features of the Cathedral Cave sediments, especially those pertaining to phosphatic and carbonate cementation. These, however, receive no further attention here as they shed no light on conditions prevailing at the time of primary deposition. The sediments are composed predominantly of resistant fabrics, namely silica (quartz grains plus minor chert), ferruginous clayey aggregates, and ferruginous quartz-clay aggregates. Silica is especially resistant to both chemical and mechanical breakdown. The ferruginous aggregates have attributes that are characteristic of weathered profiles. On the one hand, they are composed of chemically-resistant species (quartz, most probably kaolin, and iron oxides), and, on the other, they have retained sufficient mechanical strength to survive hydrodynamic transport – in some instances to the extent that some aggregate-rich beds are well-sorted (cf. some lenses in Unit 1).

In terms of their dominant primary constituents, the Cathedral Cave sediments range from essentially ‘clean’ quartz sands (cf. Unit 4 and quartz sand lenses within Unit 1) to admixtures in which ferruginous aggregates dominate over quartz (cf. Unit 2b and some lenses within Unit 1). This implies two primary sources of sediment, neither of which is simply a direct reworking of basement

formations. The most likely source of the clean quartz sands is the Quaternary dune system, after dissolution of its labile carbonate component. The Quaternary dunes were not affected by the deep weathering event that resulted in ferruginization of the Parilla Sand and the development of a lateritic, terminal weathering, surface upon it. This weathering event is not manifest as ferruginization in the Gambier Limestone, but it most likely would have affected more localized, secondary, terrigenous accumulations of insoluble residues (i.e., quartz and clay) derived from both it and the Parilla Sand.

It is conceivable that sediments from the two suggested sources became mixed while entrained, but marked facies changes, such as occur in Unit 1, suggest that there was also ‘switching’ from one primary source to another as surface hydrology changed. Even when present in relatively low abundances, the ferruginous aggregates tend to saturate the color of bulk samples, making it difficult to estimate relative proportions of quartz grains to ferruginous aggregates, and to discern smaller-scale bedding geometries in the field.

The admixtures of quartz and ferruginous aggregates range in the deposit from relatively well-sorted (cf. Unit 3 and lenses within Unit 1) to poorly-sorted sediments, as exemplified by Unit 2b, which is especially rich in ferruginous aggregates. Unit 2a and some lenses within Unit 1 are proportionally richer in quartz, but are also relatively poorly-sorted.

Overall, the relative abundance of carbonate grains and charcoal fragments appears to co-vary with the degree of sorting: the more poorly-sorted the sediment, irrespective of its composition, the higher the frequency of carbonate grains and the higher the abundance of charcoal fragments.

In terms of the theoretical considerations outlined above, these observations are consistent with the idea that more poorly-sorted sediments, with higher relative abundances of geochemically labile fabrics (i.e., carbonate grains) and higher charcoal contents, accumulated when effective precipitation was low – the natural frequency of wildfires being higher under drier conditions. The better-sorted sediments, in which carbonate grains are infrequent and charcoal is less abundant, accumulated under conditions of higher effective precipitation.

Thus, the sedimentological record of environmental change in the Cathedral Cave excavation is that Unit 4 (528 ± 41 ka) and Unit 3 (~ 290 – 280 ka) were deposited at the higher end of the effective precipitation range. Units 2b (257 ± 21 ka) and 2a (231 ± 21 ka) were deposited under conditions of significantly lower effective precipitation, followed by an amelioration during the period of deposition of Unit 1 (206 ± 16 ka).

Conclusions. It is not possible to suggest values of effective precipitation for the different periods, nor is it presently possible to constrain the amount of time-averaging involved for each of the differentiated depositional units. However, the *general* pattern recognized above, and especially for the time interval represented by Units 3–1 (making allowance for the uncertainty associated with the age determination for each unit), shows a correspondence to climatic cycling at the approximately 100-k.y. scale, as determined from other datasets (see main text).

Faunal remains from Cathedral Cave were collected in ~ 10 cm-deep spits, a scale at which the main depositional units can be compared (see main text), but which cannot resolve variation at the scale of facies changes within the units. The faunal data and sedimentological observations presented here, notwithstanding the fact that the latter are essentially qualitative, are comparable in the sense that they both show evidence of environmental change attributable to changes in effective precipitation over the same time range.

The indications are that the Cathedral Cave depositional system was relatively simple. Although modeled here in terms of the regional geology, a better understanding of the local geology would be useful. The application of suitable quantitative techniques, and more comprehensive investigation of the full suite of sediments in the Naracoorte cave system, offer prospects for paleoenvironmental information to complement the speleothem record.

REFERENCES

- Aitken M.J., 1998, *An introduction to optical dating*: Oxford University Press, Oxford.
- Ayliffe, L.K., Marianelli, P.C., Moriarty, K.C., Wells, R.T., McCulloch, M.T., Mortimer, G.E., and Hellstrom, J.C., 1998, 500 ka precipitation record from southeastern Australia: evidence for interglacial relative aridity: *Geology*, v. 26, p. 147–150.
- Bailey, R.M., 2004, Paper I—simulation of dose absorption in quartz over geological timescales and its implications for the precision and accuracy of optical dating. *Radiation Measurements*, v. 38, p. 299–310.
- Banerjee, D., Hildebrand, A.N., Murray-Wallace, C.V., Bourman, R.P., Brooke, B.P., and Blair, M., 2003, New quartz SAR-OSL ages from the stranded beach dune sequence in south-east South Australia. *Quaternary Science Reviews*, v. 22, p. 1019–1025.
- Barnosky, A.D., Bell, C.J., Emslie, S.D., Goodwin, H.T., Mead, J.I., Repenning, C.A., Scott, E., and Shabel, A.B., 2004, Exceptional record of mid-Pleistocene vertebrates helps differentiate climatic from anthropogenic ecosystem perturbations: *Proceedings of the National Academy of Sciences USA*, v. 101, p. 9297–9302.
- Barnosky, A.D., Carrasco, M.A., and Davis, E.B., 2005, The impact of the species–area relationship on estimates of paleodiversity. *PLoS Biology*, v. 3, p. e266.
- Bøtter-Jensen, L., McKeever, S.W.S., and Wintle, A.G., 2003, *Optically stimulated luminescence dosimetry*: Elsevier Science, Amsterdam, 355 p.
- Brown, C.M., and Stephenson, A.E., 1991, *Geology of the Murray Basin, southeastern Australia*. Bureau of Mineral Resources, Geology and Geophysics, Australia, Bulletin, v. 235, p. 1–430.
- Cook, P.J., Colwell, J.B., Firman, J.M., Lindsay, J.M., Schwebel, D.A., and von der Borch, C.C., 1977, The late Cainozoic sequence of southeast South Australia and Pleistocene sea-level changes. Bureau of Mineral Resources *Journal of Geology and Geophysics*, v. 2, p. 81–88.

- Bowler, J.M., Johnston, J., Olley, J.M., Prescott, J.R., Roberts, R.G., Shawcross, W., and Spooner, N.A., 2003, New ages for human occupation and climatic change at Lake Mungo, Australia: *Nature*, v. 421, p. 837–840.
- Esteban, M., and Klappa, C.F., 1983, Subaerial exposure environment. *American Association of Petroleum Geologists Memoir*, v. 33, p. 1-63.
- Galbraith, R.F., Roberts, R.G., Laslett, G.M., Yoshida, H., and Olley, J.M., 1999, Optical dating of single and multiple grains of quartz from Jinmium rock shelter, northern Australia: Part I, experimental design and statistical models. *Archaeometry*, v. 41, p. 339–364.
- Galbraith, R.F., Roberts, R.G., and Yoshida, H., 2005, Error variation in OSL palaeodose estimates from single aliquots of quartz: a factorial experiment. *Radiation Measurements*, v. 39, p. 289–307.
- Gresham, R., 2000, A palaeontological investigation of the Uranium-series dated deposit in Grant Hall Chamber, Naracoorte Caves, South Australia. [B.Sc. (Hons) thesis]: Adelaide, Flinders University, 114 p.
- Hellstrom, J.C., 2003, Rapid and accurate U/Th dating using parallel ion-counting multi-collector ICP-MS. *Journal of Analytical Atomic Spectrometry*, v. 18, p. 1346-1351.
- Johnson, C.N., and Prideaux, G.J., 2004, Extinctions of herbivorous mammals in Australia's late Pleistocene in relation to their feeding ecology: no evidence for environmental change as cause of extinction. *Austral Ecology*, v. 29, p. 553–557.
- McDowell, M.C., 2001, The analysis of Late Quaternary fossil mammal faunas from Robertson Cave (5U17, 18, 19) and Wet Cave (5U10, 11) in the Naracoorte Caves World Heritage Area, South Australia. [M.Sc. thesis]: Adelaide, Flinders University, 378 p.
- Megirian, D., Murray, P.F., Schwartz, L.R.S., and von der Borch, C.C., 2004, Late Oligocene Kangaroo Well Local Fauna from the Ulta Limestone (new name), and climate of the Miocene oscillation across central Australia. *Australian Journal of Earth Sciences*, v. 51, p. 701-741.

- Moriarty, K.C., McCulloch, M.T., Wells, R.T., and McDowell, M.C., 2000, Mid-Pleistocene cave fills, megafaunal remains and climate change at Naracoorte, South Australia: towards a predictive model using U-Th dating of speleothems: *Palaeogeography, Palaeoclimatology, Palaeoecology*, v. 159, p. 113–143.
- Olley, J.M., Pietsch, T., and Roberts, R.G., 2004, Optical dating of Holocene sediments from a variety of geomorphic settings using single grains of quartz. *Geomorphology*, v. 60, p. 337–358.
- Prescott, J.R., and Hutton, J.T., 1994, Cosmic ray contributions to dose rates for luminescence and ESR dating: large depths and long-term time variations. *Radiation Measurements*, v. 23, p. 497–500.
- Raup, D.M., 1975, Taxonomic diversity estimation using rarefaction. *Paleobiology*, v. 1, p. 333–342.
- Reed, E.H., and Bourne, S.J., 2000, Pleistocene fossil vertebrate sites of the South East region of South Australia: *Transactions of the Royal Society of South Australia*, v. 124, p. 61–90.
- Roberts, R.G., Flannery, T.F., Ayliffe, L.K., Yoshida, H., Olley, J.M., Prideaux, G.J., Laslett, G.M., Baynes, A., Smith, M.A., Jones, R., and Smith, B.L., 2001, New ages for the last Australian megafauna: continent-wide extinction about 46,000 years ago: *Science*, v. 292, p. 1888–1892.
- Schumm, S.A., 1968, Speculations concerning paleohydrologic controls of terrestrial sedimentation. *Geological Society of America Bulletin*, v. 79, p. 1573–1588.
- Strahan, R., 1995, *The mammals of Australia*: Reed New Holland, Sydney, 756 p.
- Wells, R.T., Moriarty, K.C., and Williams, D.L.G., 1984, The fossil vertebrate deposits of Victoria Fossil Cave Naracoorte: an introduction to the geology and fauna: *The Australian Zoologist*, v. 21, p. 305–333.
- Wroe, S., Argot, C., and Dickman, C.R., 2004, On the rarity of big fierce carnivores and primacy of isolation and area: tracking large mammalian carnivore diversity on two isolated continents. *Proceedings of the Royal Society of London B*, v. 271, p. 1203–1211.